Int J Adv Manuf Technol (2017) 91:1355–1368
DOI 10.1007/s00170-016-9810-y

ORIGINAL ARTICLE

Effects of pouring temperature on microstructure, mechanical properties, and fracture behavior of Al/Mg bimetallic composites produced by lost foam casting process

Guangyu Li[1] · Wenming Jiang[1] · Zitian Fan[1] · Zailiang Jiang[1] · Xinwang Liu[1] · Fuchu Liu[1]

Received: 31 July 2016 / Accepted: 21 November 2016 / Published online: 7 December 2016

Abstract In the present work, the Al/Mg bimetallic composites were produced using lost foam casting (LFC) process, and the effects of the pouring temperature on the microstructure, mechanical properties, and fracture behavior of the Al/Mg bimetallic composites produced by the LFC process were investigated in order to obtain an optimized bonding between aluminum alloy and magnesium alloy. It was found that the pouring temperature had a significant effect on the interface between the aluminum and the magnesium. With increasing pouring temperature, the thickness of the interface layer obviously increased. When the pouring temperature was 730 °C, a compact and uniform interface layer was obtained between the aluminum and the magnesium. The interface layers of the Al/Mg bimetallic composites obtained with different pouring temperatures primarily consisted of three different reaction layers, namely $Al_{12}Mg_{17}$ + δ-Mg eutectic, $Al_{12}Mg_{17} + Mg_2Si$, and $Al_3Mg_2 + Mg_2Si$. The interface layers of the Al/Mg bimetallic composites with different pouring temperatures had higher microhardnesses compared to the base metals. The Al/Mg bimetallic composite with the pouring temperature of 730 °C obtained a maximum shear strength due to its superior interface, showing an optimized bonding between the aluminum and the magnesium. The SEM fractograph of the bimetallic composite mostly exhibited a brittle fracture morphology, and the $Al_{12}Mg_{17}$ + δ-Mg eutectic partly generated a plastic deformation.

Keywords Lost foam casting · Al/Mg bimetallic composites · Pouring temperature · Microstructure · Mechanical properties · Fracture behavior

1 Introduction

Currently, magnesium and aluminum alloys are widely applied in vehicle construction and aerospace industries in order to improve the energy efficiency [1–4]. However, sometimes, one of these alloys alone is difficult to meet the demands of the integrated performance because of their characteristics. It is well known that the magnesium alloy has many advantages including low density, good electromagnetic shielding capacity, and machinability, but poor ductility and corrosion resistance. In contrast, the aluminum alloy has good plastic and admirable corrosion resistance, while its density is relatively higher than that of the magnesium alloy [5–7]. Thus, the dissimilar joint between the magnesium alloy and the aluminum alloy may be a promising solution for the industrial applications, as the Al/Mg bimetallic composites combine some expected properties that cannot be fully supplied by a single material [8, 9].

There are a large number of methods to prepare the Al/Mg bimetallic composites, such as rolling bonding [10], gas metal arc plug welding [11], diffusion welding [12], friction stir welding [13–16], resistance spot welding [17, 18], transfer welding [19], laser welding [20, 21], and compound casting [22]. In general, the rolling method is mainly applied in the layered material or the strip material, which is difficult to prepare complex parts. Similarly, the welding methods cannot be used to prepare the bimetallic parts with a complex shape,

✉ Wenming Jiang
jwenming@163.com; wmjiang@hust.edu.cn

✉ Zitian Fan
fanzt@mail.hust.edu.cn

[1] State Key Laboratory of Material Processing and Die & Mould Technology, School of Material Science and Engineering, Huazhong University of Science and Technology, Wuhan 430074, China

and the bonding interface obtained by the welding method generally contains a higher stress, thereby results in cracking. The sand casting process is difficult to satisfy the dimensional precision and surface roughness of the bimetallic composites.

The lost foam casting (LFC) process has been regarded as a near-net-shape casting technology, which has many advantages such as high precision, low surface roughness, flexible structure design, and low cost [23–26]. Recently, the LFC process has been considered as an attractive method to fabricate the Al/Mg bimetallic composites by use of assembling a solid part inside the foam pattern prior to pouring, because it can take the advantages of the LFC process to prepare the Al/Mg bimetallic composites. Furthermore, the reduction gas generating from the evaporation of the foam pattern can protect the surface of aluminum and magnesium alloys from oxidation, as pointed out by the literatures [27, 28]. However, the investigations with respect to the preparation of the Al/Mg bimetallic composites produced using the LFC process are relatively less in the present reports [29, 30]. During the fabrication process of the Al/Mg bimetallic composites, the pouring temperature is of importance to obtain an excellent bonding between the aluminum and the magnesium. Unfortunately, there is also an unexplored area related to its investigation, and how to obtain an excellent metallurgical bonding between the aluminum and the magnesium is still a challenge during the LFC process.

In this study, the Al/Mg bimetallic composites were produced using the LFC process, and the effects of the pouring temperature on the microstructure, mechanical properties, and fracture behavior of the Al/Mg bimetallic composites were investigated in order to establish an optimized bonding between the aluminum alloy and the magnesium alloy. Additionally, the formation mechanism of the interface of the Al/Mg bimetallic composites was also discussed.

2 Experimental procedures

The A356 aluminum alloy and AZ91D magnesium alloy were respectively used as a solid insert and a melt, and their compositions are shown in Tables 1 and 2. The foam pattern was made of the expanded polystyrene material.

The cylindrical aluminum inserts were cut from the A356 aluminum alloy ingot by use of an electrical discharge machine, whose diameter and height were 10 and 130 mm, respectively. The surfaces of the aluminum inserts were then polished with silicon carbide papers prior to rinsing. Afterwards, the aluminum inserts were assembled inside the foam patterns. The foam patterns together with the aluminum inserts were finally immersed into a water-based refractory slurry and then dried in an oven at 50 °C.

Table 1 Chemical composition of A356 (wt.%)

Material	Mass fraction (%)				
A356	Si	Mg	Ti	Fe	Al
	6.81	0.439	0.017	0.205	Bal.

Table 2 Chemical composition of AZ91D (wt.%)

Material	Mass fraction (%)			
AZ91D	Al	Zn	Mn	Mg
	9.08	0.62	0.23	Bal.

The schematic illustration of the experimental equipment is presented in Fig. 1. First, the foam patterns together with the aluminum inserts were put into a sand flask, which was successively filled with unbonded loose sand and compacted by a three-dimensional vibration table. The plastic film was then covered on the top of the sand flask. Finally, a sprue cup was placed on the sprue prior to pouring. The AZ91D magnesium alloy was put into a stainless steel crucible to melt in an electrical resistance furnace. The pouring temperatures of the molten magnesium metal used in this study were 710, 730, and 750 °C, respectively, and the vacuum level was 0.03 MPa.

In order to investigate the influence of the pouring temperature on the interface between the aluminum insert and the magnesium melt, a simulation software was used to analyze the time and the temperature of the Mg melt arriving at the different positions of the surface of the Al insert, as shown in Fig. 2.

Metallographic samples were first machined from the middle position of the Al/Mg bimetallic composites, which were then etched using a 4% nital solution after grinding and polishing. A Quanta 400 scanning electron microscope equipped with an energy-dispersive X-ray spectroscopy

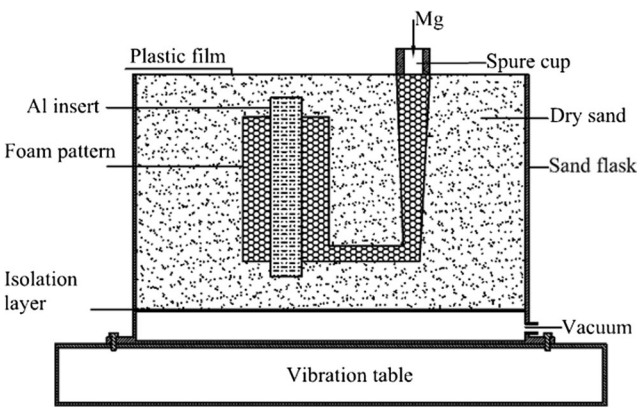

Fig. 1 Schematic illustration of the experimental equipment

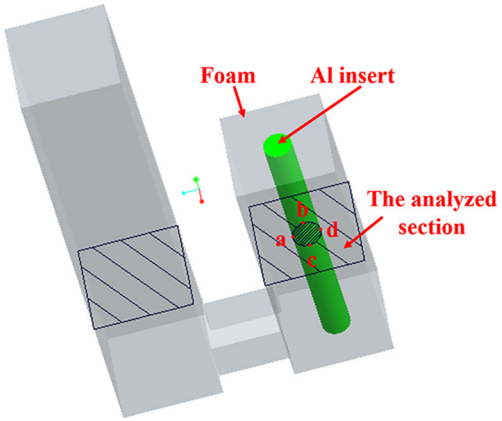

Fig. 2 Schematic diagram of the positions analyzed by the simulation

(EDS) was used to observe the characteristics of microstructure at the interface zones and quantitatively analyze the compositional variations of the interface between the aluminum and the magnesium.

The microhardnesses of the interface of the Al/Mg bimetallic composites were measured using a TWVS-1 hardness tester. The push-out tests were performed using a Zwick Z100 universal testing machine with a crosshead displacement rate of 0.5 mm/min in order to determine the shear strength of the Al/Mg bimetallic composites. At least three samples for each pouring temperature were used to perform the push-out test in order to minimize the errors. Figure 3 illustrates a schematic diagram of the push-out test. The fractured surfaces of the push-out samples were finally observed and analyzed using the SEM and EDS methods.

3 Results

3.1 Microstructures of the interface layer of the Al/Mg bimetallic composites

Figure 4 shows the SEM micrographs of the Al/Mg bimetallic composites with different pouring temperatures. As can be seen, the pore defects with a large size are apparently present at the interface layer of the Al/Mg bimetallic composite with a pouring temperature of 710 °C, as shown in Fig. 4b. With a pouring temperature of 730 °C, a compact and uniform interface layer can be observed, as shown in Fig. 4c. Increasing pouring temperature to 750 °C, the thickness of the interface layer clearly exhibits an inhomogeneous morphology, as shown in Fig. 4d, e.

In addition, the thicknesses of the interface layers of the Al/Mg bimetallic composites were measured with the Image software. The results show that the average thickness of the interface layer is about 1440 μm with a pouring temperature of 710 °C. Increasing pouring temperature to 730 °C, the average thickness of the interface layer slightly increases up to about 1480 μm. Further increasing pouring temperature to 750 °C, the thickest part of the interface layer reaches approximately 2650 μm. These results suggest that the pouring temperature has a significant effect on the thickness of the interface layer of the Al/Mg bimetallic composites.

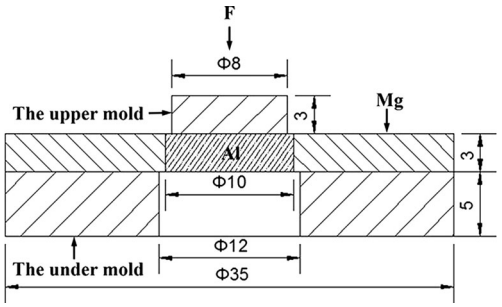

Fig. 3 Schematic diagram of the push-out test (unit: mm)

3.2 Phase compositions of the interface layer of the Al/Mg bimetallic composites

Tables 3, 4, and 5 respectively list the quantitative analysis results of the Al and Mg elements in different areas of the interface layers from different pouring temperatures. It was found that the interface layers can be divided into three different reaction layers for all the samples with different pouring temperatures. The reaction layer I close to the magnesium base is primarily composed of the $Al_{12}Mg_{17}$ + δ-Mg eutectic due to the eutectic transformation, and the Al_3Mg_2 phase is a main constituent of the layer III near to the aluminum base. The ratio of the Al and Mg elements for different areas of the layer II is not constant. Considering the relatively wide range of the composition for the $Al_{12}Mg_{17}$ phase in the Al-Mg binary phase diagram shown in Fig. 5, it suggests that the middle layer II is primarily composed of the $Al_{12}Mg_{17}$ phase, which is consistent with the other studies [33, 34]. These results indicate that the pouring temperature has little effect on the compositions of the interface layer.

Figures 6, 7, and 8 show the EDS maps of the interface zones of the Al/Mg bimetallic castings with different pouring temperatures. As can be seen, the composition distributions of the Al, Mg, and Si elements are clearly observed at the reaction layer between the aluminum and the Mg for all the samples, showing that the rule of the distributions of the elements is uniform. The Mg element distributes gradually from the magnesium side to the aluminum side, while the distributions of the Al element are just opposite to the Mg element. The Si element also exists at the interface layer zones, because the Si element that existed in the A356 aluminum alloy distributes to the Mg side.

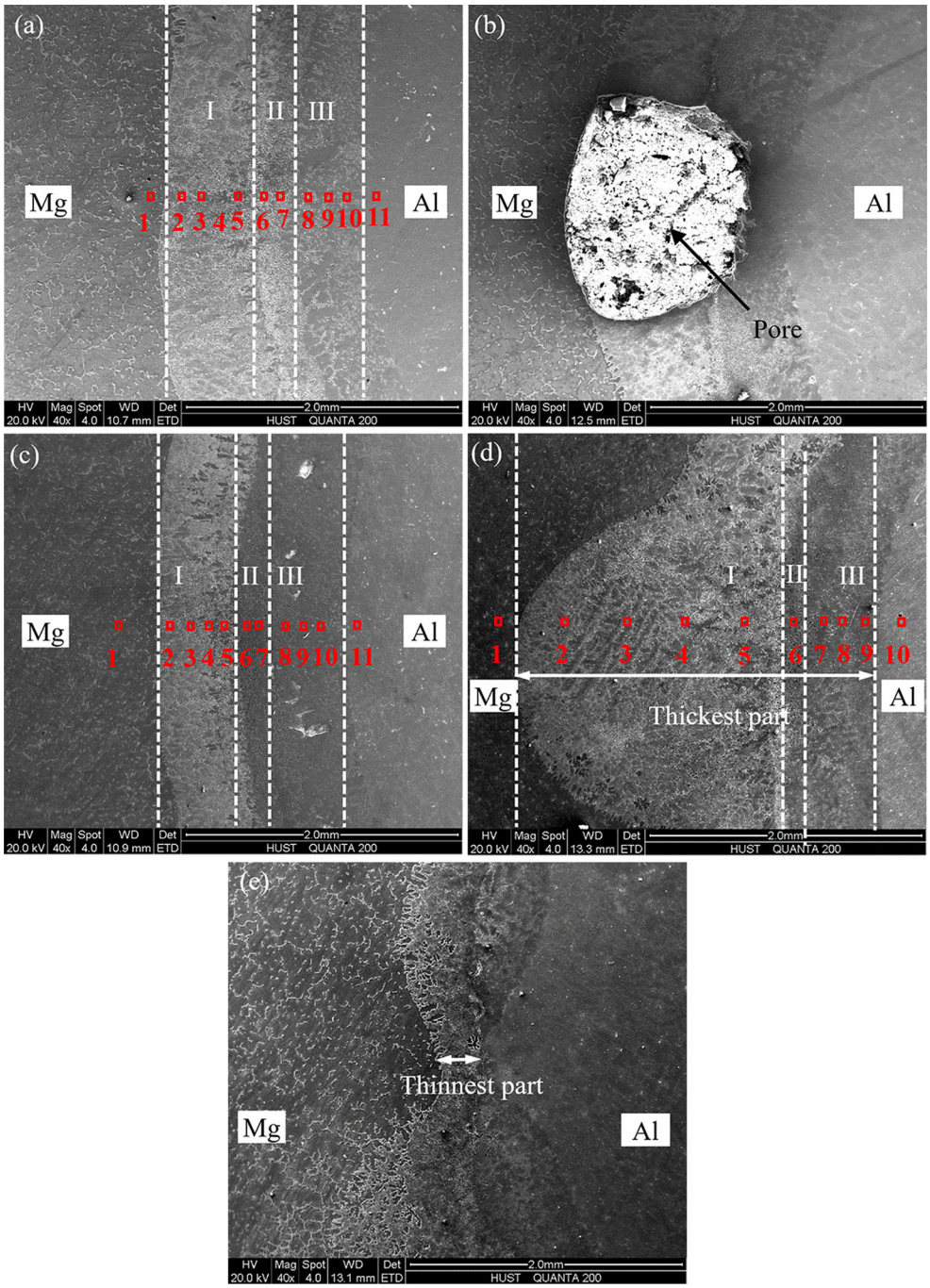

Fig. 4 SEM micrographs of the interface layer of the Al/Mg bimetallic composites with different pouring temperatures: **a** 710 °C, **b** pore defect of 710 °C, **c** 730 °C, **d** the thickest part of 750 °C, and **e** the thinnest part of 750 °C

More detailed observations and compositional analysis of the interfacial microstructures with different pouring temperatures are shown in Fig. 9 (I, II, and III are respectively corresponding to reaction layers I, II, and III shown in Fig. 4) and Table 6. It is obvious that the SEM micrographs of the interfacial microstructures with different pouring temperatures at different areas of the interfaces almost show a similar morphology. It is also further confirmed that the layers I, II, and III primarily consist of the $Al_{12}Mg_{17}$ + δ-Mg eutectic, $Al_{12}Mg_{17}$, and Al_3Mg_2 intermetallics, respectively. Moreover, the Mg_2Si phase is also detected in the layers II and III of the interfacial microstructures with different pouring temperatures.

3.3 Mechanical properties of the Al/Mg bimetallic composites

The microhardness distributions of the interface zones of the Al/Mg bimetallic composites with different pouring

Table 3 EDS analysis results of Al and Mg elements at the Al/Mg interface corresponding to areas indicated in Fig. 4a

Area no.	Element compositions (at.%)		Element compositions ratio (Al/Mg)	Inference component
	Al	Mg		
1	12.29	87.71	–	Mg
2	36.16	63.84	0.57	$Al_{12}Mg_{17}$ + δ-Mg
3	36.15	63.85	0.57	$Al_{12}Mg_{17}$ + δ-Mg
4	33.66	66.34	0.51	$Al_{12}Mg_{17}$ + δ-Mg
5	37.98	61.9	0.61	$Al_{12}Mg_{17}$ + δ-Mg
6	48.98	51.02	0.96	$Al_{12}Mg_{17}$
7	46.52	53.48	0.87	$Al_{12}Mg_{17}$
8	58.97	41.03	1.47	Al_3Mg_2
9	60.84	39.16	1.55	Al_3Mg_2
10	60.83	39.17	1.55	Al_3Mg_2
11	98.89	1.01	–	Al

temperatures are shown in Fig. 10. It can be observed that the microhardness distributions at the interface zones of the Al/Mg bimetallic composites with different pouring temperatures basically exhibit a same trend. The reaction layers at the interfaces have higher microhardnesses compared to the base metals, which implies that the rigid and brittle phases such as Al_3Mg_2 and $Al_{12}Mg_{17}$ have been generated at the interface of the Al/Mg bimetallic composites. And, the Al_3Mg_2 phase has the highest microhardness at the interface.

Figure 11 presents the results of the push-out tests. As can be seen, the Al/Mg bimetallic composite with a pouring temperature of 730 °C obtains a maximum shear strength up to 47.67 MPa compared to those of the 710 and 750 °C, due to a better interface between the aluminum and the magnesium. When the pouring temperature is 710 °C, the Al/Mg bimetallic composite has a poor shear strength.

Figure 12 shows SEM fractographs and EDS analysis of the Al/Mg bimetallic composites obtained by different pouring temperatures. It is clear that the SEM fractographs of the bimetallic composites with different pouring temperatures mostly exhibit a brittle fracture morphology, and a larger number of cleavage planes are observed on the fracture surfaces, especially in the fracture surface of the Al/Mg bimetallic composite with the pouring temperature of 750 °C. According to the EDS analysis results, it reveals that the cleavage planes are mainly the brittle and hardness $Al_{12}Mg_{17}$ and Al_3Mg_2 intermetallics, as shown in Fig. 12a, c. Furthermore, the gap and pore defects are obviously

Table 4 EDS analysis results of Al and Mg elements at the Al/Mg interface corresponding to areas indicated in Fig. 4c

Area no.	Element compositions (at.%)		Element compositions ratio (Al/Mg)	Inference component
	Al	Mg		
1	10.82	89.18	–	Mg
2	32.26	67.74	0.48	$Al_{12}Mg_{17}$ + δ-Mg
3	37.06	62.94	0.59	$Al_{12}Mg_{17}$ + δ-Mg
4	38.19	61.81	0.62	$Al_{12}Mg_{17}$ + δ-Mg
5	36.26	63.74	0.51	$Al_{12}Mg_{17}$ + δ-Mg
6	48.57	51.43	0.94	$Al_{12}Mg_{17}$
7	49.35	50.65	0.97	$Al_{12}Mg_{17}$
8	58.23	41.77	1.39	Al_3Mg_2
9	60.25	39.75	1.52	Al_3Mg_2
10	62.08	37.92	1.64	Al_3Mg_2
11	98.85	1.15	–	Al

Table 5 EDS analysis results of Al and Mg elements at the Al/Mg interface corresponding to areas indicated in Fig. 4d

Area no.	Element compositions (at.%)		Element compositions ratio (Al/Mg)	Inference component
	Al	Mg		
1	12.76	87.24	–	Mg
2	34.69	65.31	0.53	$Al_{12}Mg_{17}$ + δ-Mg
3	36.36	63.64	0.57	$Al_{12}Mg_{17}$ + δ-Mg
4	36.27	63.73	0.57	$Al_{12}Mg_{17}$ + δ-Mg
5	33.19	66.81	0.50	$Al_{12}Mg_{17}$ + δ-Mg
6	41.68	56.21	0.74	$Al_{12}Mg_{17}$
7	55.57	41.33	1.34	Al_3Mg_2
8	56.55	40.31	1.40	Al_3Mg_2
9	57.99	38.43	1.51	Al_3Mg_2
10	98.79	1.21	–	Al

observed in the fracture surface of the Al/Mg bimetallic composite with the pouring temperature of 710 °C, meaning that the fracture path may preferentially go through the porosity defects, which leads to a sharp decrease of the bonding strength. Additionally, in the fracture surface of the Al/Mg bimetallic composite with the pouring temperature of 730 °C, it can be seen that there are fewer cleavage planes compared to 710 and 750 °C, especially 750 °C; meanwhile, the $Al_{12}Mg_{17}$ + δ-Mg eutectic close to the magnesium base partly occurs a plastic deformation, as shown in Fig. 12b, which is benefit to the improvement of the bonding strength of the Al/Mg bimetallic composites.

4 Discussion

4.1 Formation mechanism of the interface of the Al/Mg bimetallic composites

The formation mechanism of the interface of the Al/Mg bimetallic composites obtained by the LFC process can

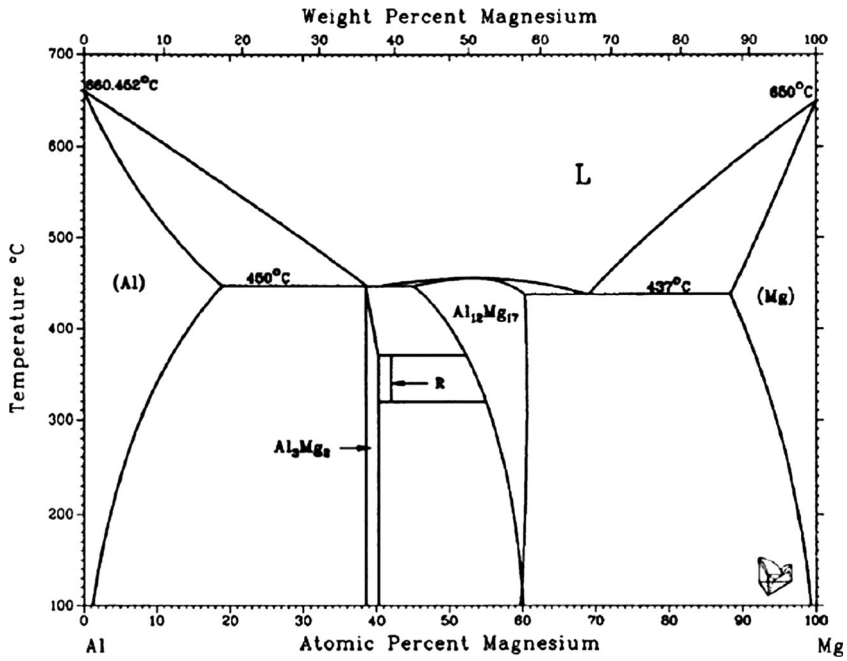

Fig. 5 Al-Mg binary phase diagram [31, 32]

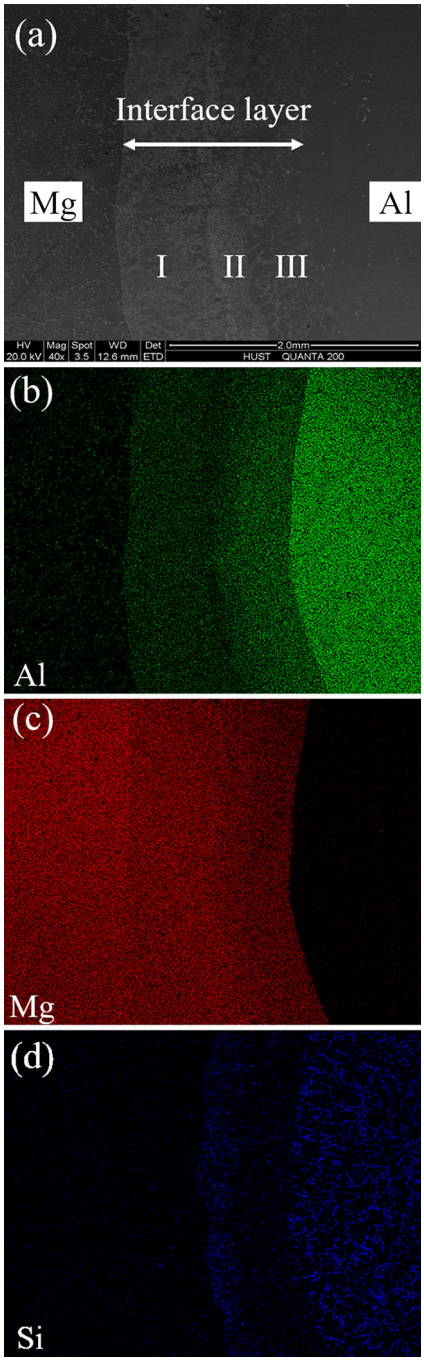

Fig. 6 EDS maps of the interface zones of the Al/Mg bimetallic castings with the pouring temperature of 710 °C: **a** SEM micrograph, **b** Al distribution map, **c** Mg distribution map, and **d** Si distribution map

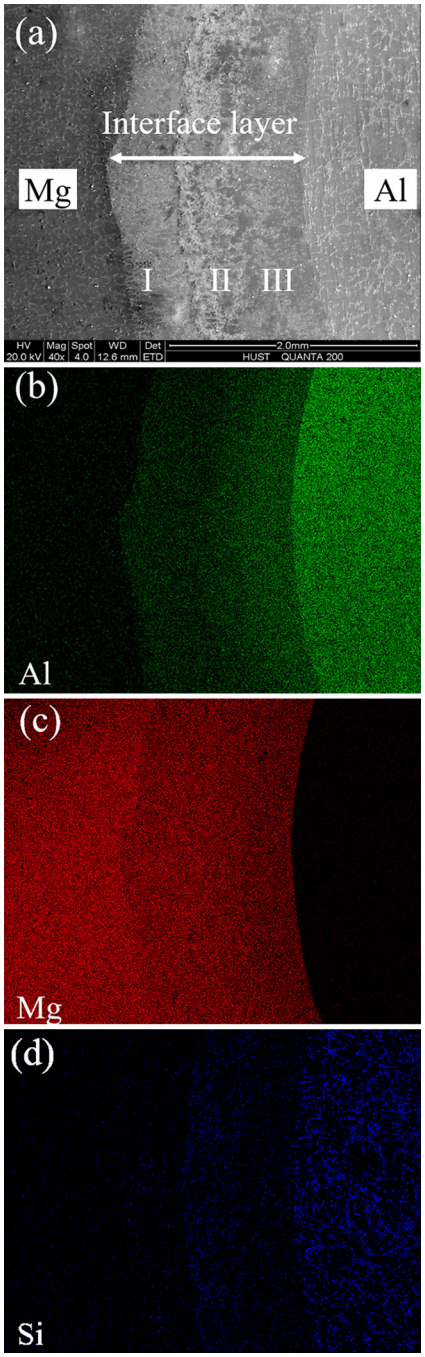

Fig. 7 EDS maps of the interface zones of the Al/Mg bimetallic castings with the pouring temperature of 730 °C: **a** SEM micrograph, **b** Al distribution map, **c** Mg distribution map, and **d** Si distribution map

be explained using the fusion bonding and diffusion bonding, as shown in Fig. 13. When the magnesium melt is poured into the foam pattern, the foam pattern quickly melts and partly evaporates due to the heat capacity from the magnesium melt. The decomposition products finally escape through the coating layer. Figure 14 shows the relation between the time and the temperature of the Mg melt arriving at the different

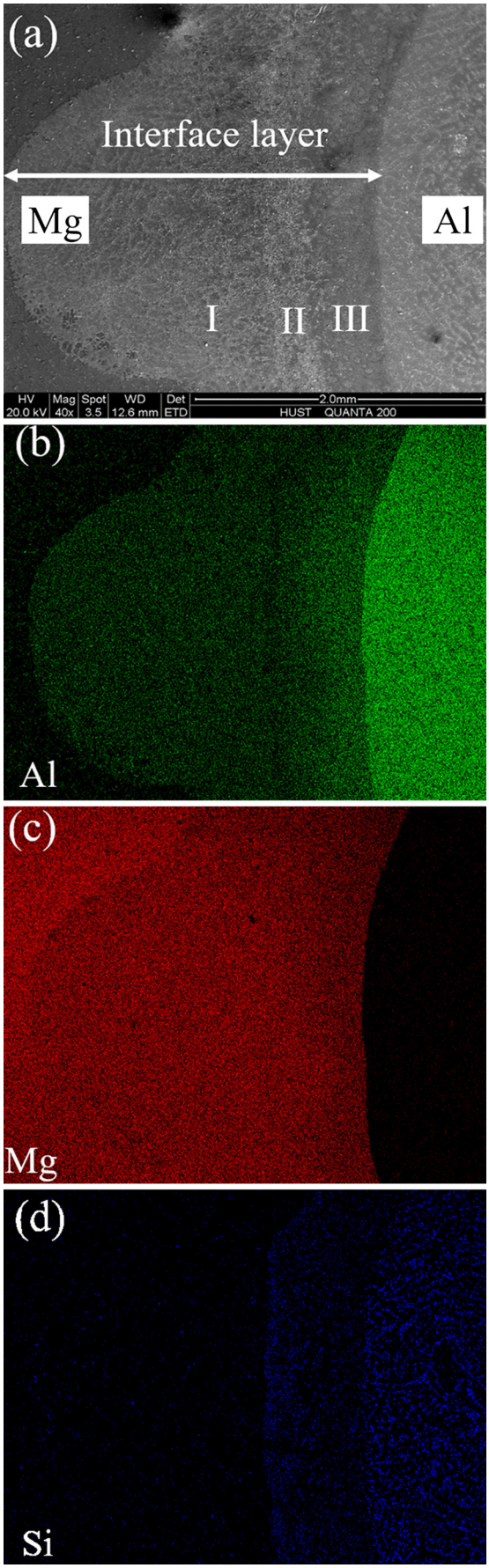

◀ **Fig. 8** EDS maps of the interface zones of the Al/Mg bimetallic castings with the pouring temperature of 750 °C: **a** SEM micrograph, **b** Al distribution map, **c** Mg distribution map, and **d** Si distribution map

positions of the surface of the Al insert under different pouring temperatures obtained by the simulation software. As can be seen, the temperature of the magnesium melt contacting with the Al insert ranges from 594 to 616 °C, and the surface of the aluminum insert may melt, thereby forms a molten pool of the melt aluminum alloy mixing with the molten magnesium alloy. In this case, the diffusion reactions occur among the molten pool, aluminum insert, and magnesium melt, resulting in the concentration gradient of the Al, Mg, and Si elements. As a result, the interface layer that primarily consists of $Al_{12}Mg_{17}$, Al_3Mg_2, and Mg_2Si intermetallic between the aluminum and the magnesium is finally formed during the solidification process.

4.2 The effects of pouring temperature on the microstructures and mechanical properties of the Al/Mg bimetallic composites

In the present work, the existence of pore defect at the interface layer is probably attributed to two reasons in the following. On the one hand, it is very important that the decomposition product of the foam materials quickly escapes through the coating layer for obtaining superior castings with no defects during the LFC process. With the decline of pouring temperature, the fluidity and filling speed of the Mg melt decrease. At the same time, the low pouring temperature goes against offsetting the heat loss on account of the foam decomposition. As a consequent, the decomposition products are difficult to escape through the coating layer before solidification, which are easy to gather around the Al insert, resulting in the formation of the pore defect or the oxide film defect. On the other hand, the viscosity of the Mg melt increases with the decrease of pouring temperature, which leads to the decrease of the rising speed of the decomposition product from the foam materials, thereby forms a few pores at the interface layer of the Al/Mg bimetallic casting with the pouring temperature of 710 °C.

In contrast, as the pouring temperature increases, the decomposition products are easy to escape through the coating layer before solidification so that there are no pores in the interface layer. However, an excessive pouring temperature will significantly promote the reaction process and diffusion process between the aluminum and the magnesium, leading to rapid increase of the thickness of the interface layer. Besides, it is easy to cause

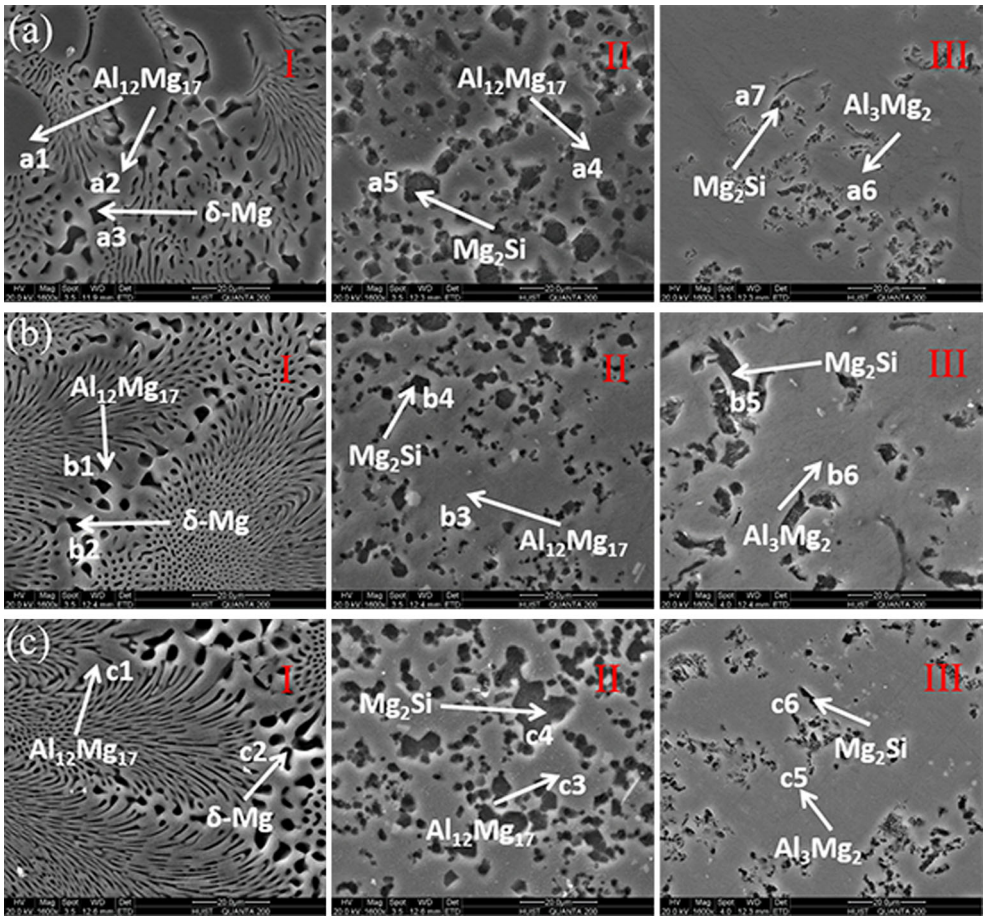

Fig. 9 High-magnification SEM micrographs of the Al/Mg interfaces with different pouring temperatures: **a** 710, **b** 730, and **c** 750 °C

turbulence during the filling process of the magnesium melt in this case, resulting in the variations of the temperature and time of the magnesium melt contacting with the aluminum insert. As a result, the diffusion

Table 6 EDS analysis results of the Al/Mg interfaces corresponding to points indicated in Fig. 9

Area no.	Pouring temperature (°C)	Layer code	Element compositions (at.%)			Element compositions ratio (Al/Mg)	Element compositions ratio (Mg/Si)	Inference component
			Al	Mg	Si			
a1	710	I	39.99	60.01	–	0.67	–	$Al_{12}Mg_{17}$
a2			41.07	58.93	–	0.70	–	$Al_{12}Mg_{17}$
a3			19.37	80.63	–	–	–	δ-Mg
a4		II	49.25	50.57	0.97	0.97	–	$Al_{12}Mg_{17}$
a5			10.99	58.71	30.30	–	1.94	Mg_2Si
a6		III	61.61	38.39	–	1.60	–	Al_3Mg_2
a7			18.44	55.00	26.56	–	2.07	Mg_2Si
b1	730	I	38.92	61.08	–	0.64	–	$Al_{12}Mg_{17}$
b2			14.48	85.52	–	–	–	δ-Mg
b3		II	44.28	55.72	–	0.79	–	$Al_{12}Mg_{17}$
b4			6.61	66.3	27.09	–	2.45	Mg_2Si
b5		III	55.47	44.53	–	1.25	–	Al_3Mg_2
b6			12.09	63.1	24.81		2.54	Mg_2Si
c1	750	I	38.44	61.56	–	0.62	–	$Al_{12}Mg_{17}$
c2			14.22	85.78	–	–	–	δ-Mg
c3		II	45.36	54.64	–	0.83	–	$Al_{12}Mg_{17}$
c4			10.28	58.36	31.36	–	1.86	Mg_2Si
c5		III	55.78	44.22	–	1.26	–	Al_3Mg_2
c6			14.25	55.72	30.03	–	1.86	Mg_2Si

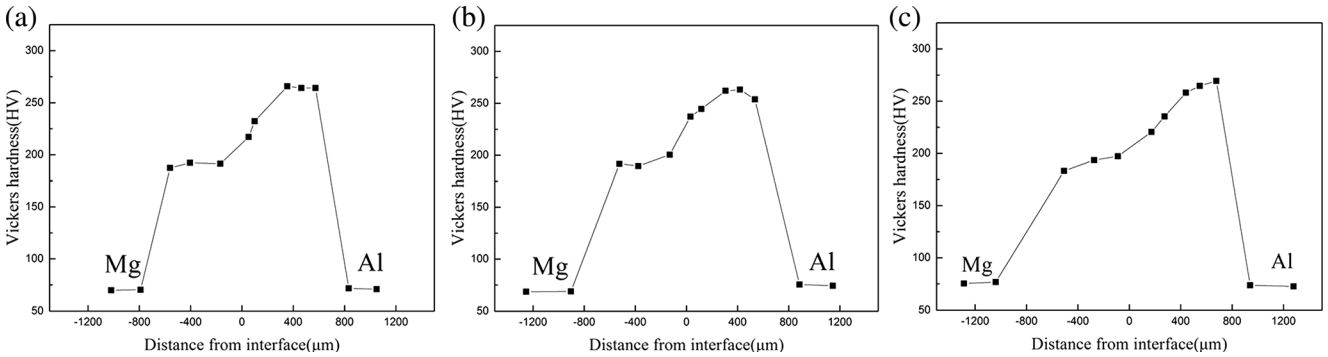

Fig. 10 Microhardness distributions of the interface zones of the Al/Mg bimetallic composites with different pouring temperatures: **a** 710, **b** 730, and **c** 750 °C

distances of the elements are different so that the thickness of the interface layer at different zones is non-uniform.

Furthermore, it can also be seen from Fig. 14 that the Mg melt first arrives at the point a and finally reaches the point d because of the special filling rule of the LFC process. The times and temperatures of the Mg melt arriving at the four points of the Al insert have smaller difference for the pouring temperatures of 710 and 730 °C. For the comparison, when the pouring temperature is up to 750 °C, the temperature of the point b is the highest and reaches 616.35 °C, which is 16.77 °C higher than that of the point d; meanwhile, the time interval of the Mg melt from the point a to the point d is also the longest, which makes the diffusion at different positions greatly vary, leading to the uneven interface layer. The results of the simulation are in good agreement with the previous theoretical analysis. Consequently, an appropriate pouring temperature is of importance to obtain a uniform and compact interface for the Al/Mg bimetallic castings obtained by the LFC process.

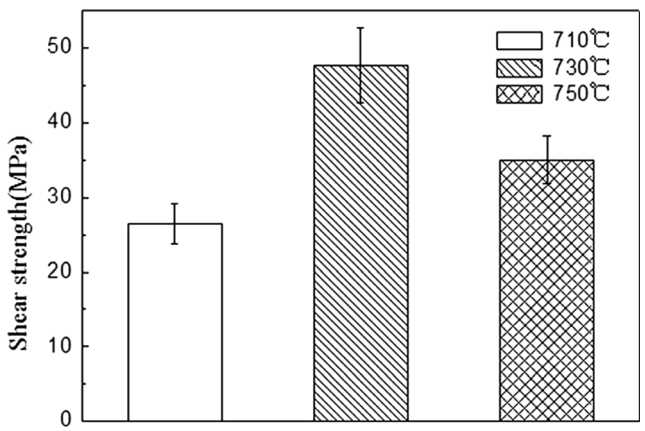

Fig. 11 Effect of the pouring temperature on the shear strength of the Al/Mg bimetallic composites

The shear strength of the Al/Mg bimetallic composites is mainly related to two factors including the existence of pores in the interface and the thickness of the interface layer. The existence of pores in the interface makes the Al and Mg no contact with each other well and destroys the integrity of the interface layer, as well as causes a stress concentration, sharply decreasing the mechanical strength of the Al/Mg bimetallic composites. On the other hand, increasing the thickness of the interface layer will reduce the bonding strength of the Al/Mg bimetallic composites because the thicker interface layer may contain more rigid and brittle intermetallics such as $Al_{12}Mg_{17}$ and Al_3Mg_2. Here, it should be noted that the pore defects have a much bigger effect on the bonding strength of the Al/Mg bimetallic composites compared to the thickness of the interface layer. According to Fig. 4, when the pouring temperatures are 730 and 750 °C, the interface layers of the Al/Mg bimetallic composites are compact, while there are some pores in the interface layer of the Al/Mg bimetallic composite with the pouring temperature of 710 °C, so the shear strengths of the samples with the pouring temperatures of 730 and 750 °C are higher than that of 710 °C. What is more, a thicker and non-uniform interface layer is obtained with the pouring temperature of 750 °C compared to 730 °C; thus, the Al/Mg bimetallic composite with the pouring temperature of 730 °C obtains a superior shear strength. In view of these investigations, it suggests that the pouring temperature has a significant effect on the microstructure and mechanical properties of the Al/Mg bimetallic composites during the LFC process. In the future, we will focus on the effects of other parameters on the microstructure and mechanical properties of the Al/Mg bimetallic composites as well as the controls of the pore defects and the thickness of the interface layer.

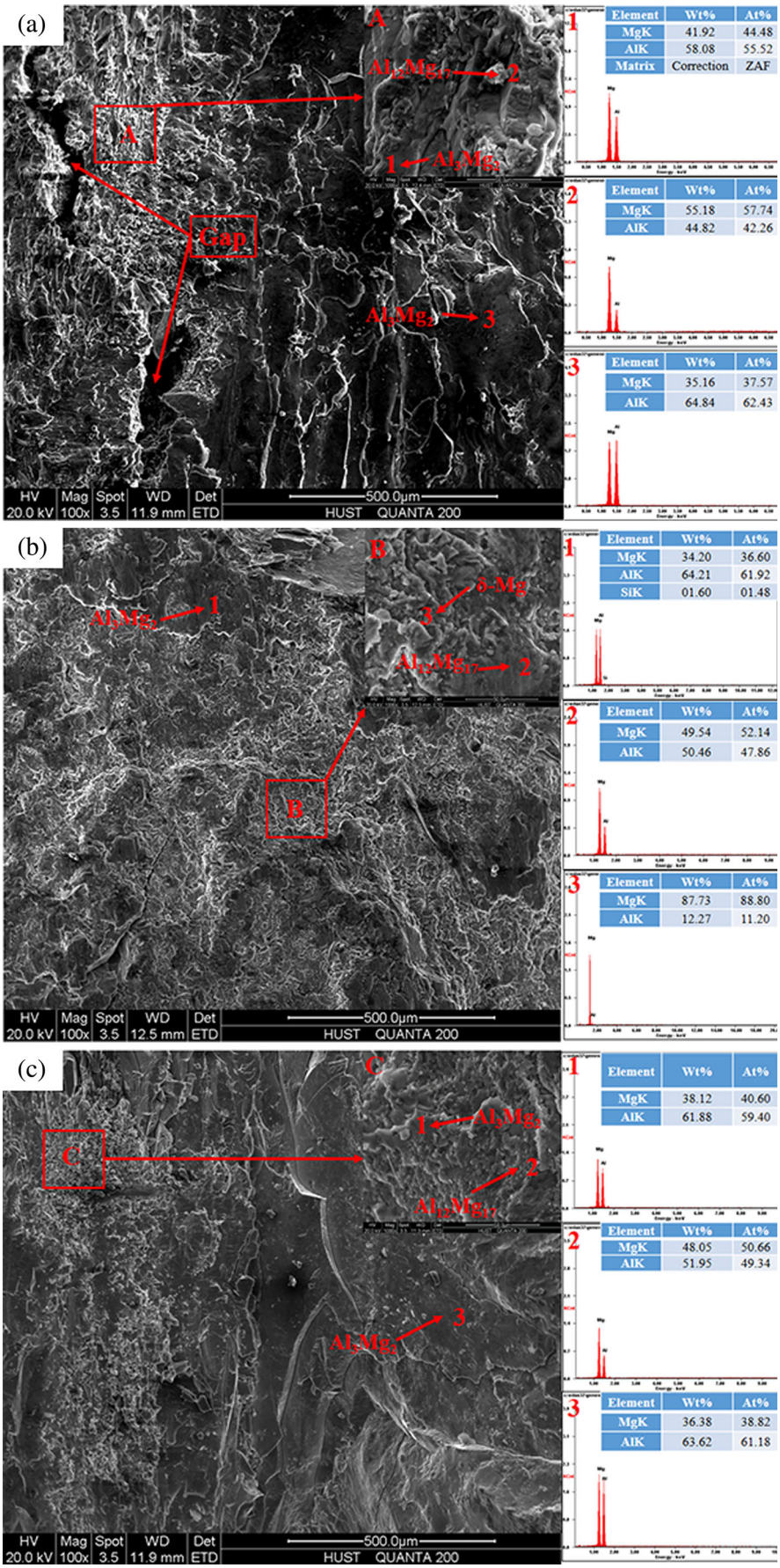

Fig. 12 SEM fractographs and EDS analysis of the Al/Mg bimetallic composites with different pouring temperatures: **a** 710, **b** 730, and **c** 750 °C

5 Conclusions

1. The pouring temperature had a great effect on the interface between the aluminum and the magnesium. With increasing pouring temperature, the thickness of the interface layer significantly increased. A compact and uniform interface layer was obtained with the pouring temperature of 730 °C.
2. The interface layers of the Al/Mg bimetallic composites with different pouring temperatures primarily consisted of three reaction layers: $Al_{12}Mg_{17}$ + δ-Mg eutectic, $Al_{12}Mg_{17}$ + Mg_2Si, and Al_3Mg_2 + Mg_2Si.
3. The interface layers of the Al/Mg bimetallic composites with different pouring temperatures had higher microhardnesses compared to the base metals, especially the Al_3Mg_2 phase, which indicated that the rigid and brittle phases have been generated at the interface of the Al/Mg bimetallic composites.
4. The Al/Mg bimetallic composite with the pouring temperature of 730 °C obtained a maximum shear strength up to 47.67 MPa, showing an optimized bonding between the aluminum and the magnesium. The SEM fractograph of the bimetallic composite mostly exhibited a brittle fracture morphology, and the $Al_{12}Mg_{17}$ + δ-Mg eutectic partly occurred a plastic deformation.

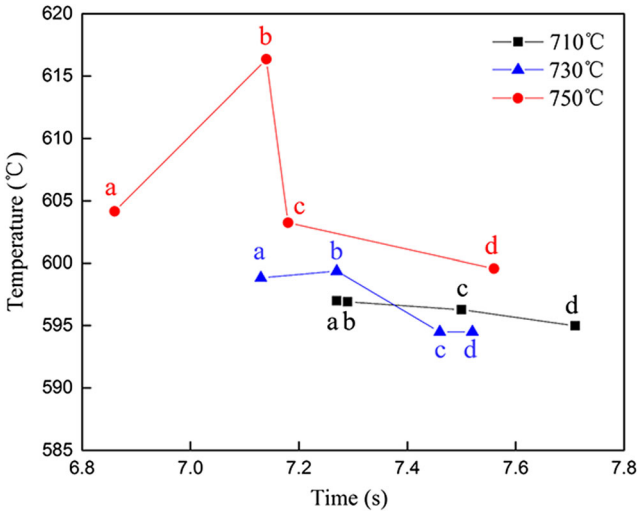

Fig. 14 The times and temperatures of the Mg melt firstly contacting with the different positions of the surface of the Al insert under different pouring temperatures (*a*, *b*, *c*, and *d*, respectively, corresponding to *a*, *b*, *c*, and *d* indicated in Fig. 2)

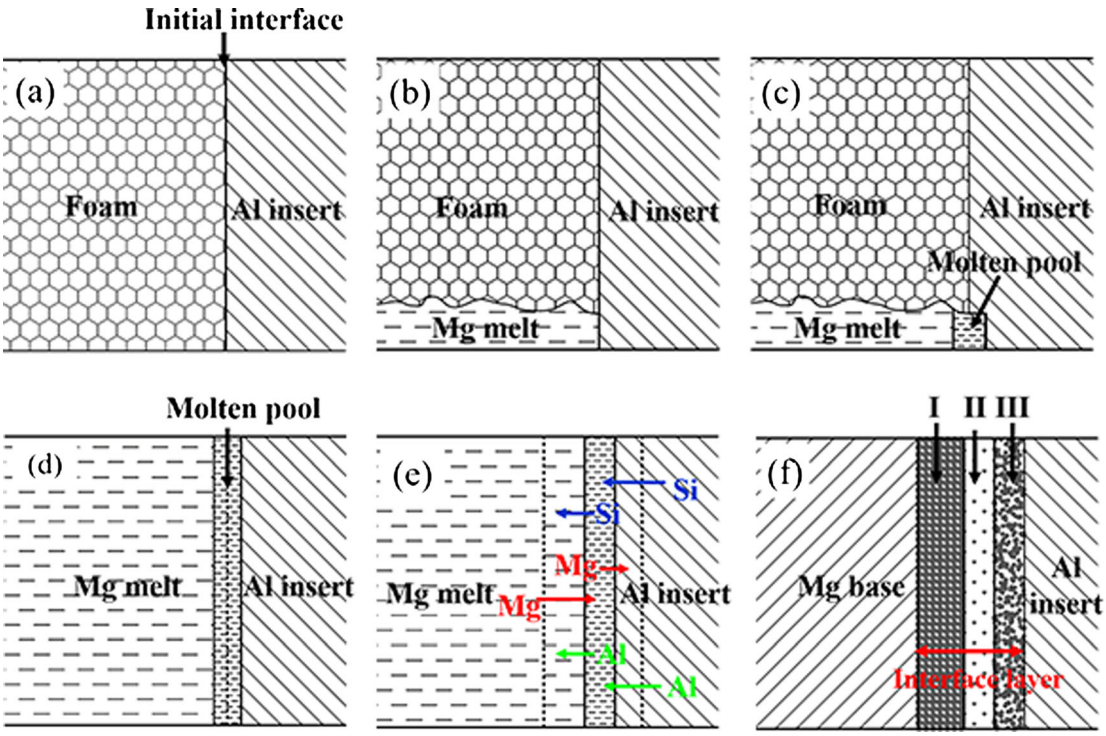

Fig. 13 The formation mechanism of the interface layer of the Al/Mg bimetallic composites: **a** before the pouring, **b** foam decomposed, **c** molten pool generated, **d** mold filling finished, **e** elements diffused, and **f** interface layer formed

Acknowledgements This work was funded by Project 51204124 supported by the National Natural Science Foundation of China, Project P2015-09 supported by the State Key Laboratory of Materials Processing and Die & Mould Technology, HUST, and Project 2015MS053 supported by the Fundamental Research Funds for the Central Universities. The authors would also like to thank the support of the Research Project of State Key Laboratory of Materials Processing and Die & Mould Technology and the Analytical and Testing Center, HUST.

References

1. Wen JL, Yang YK, Jeng MC (2009) Optimization of die casting conditions for wear properties of alloy AZ91D components using the Taguchi method and design of experiments analysis. Int J Adv Manuf Technol 41:430–439. doi:10.1007/s00170-008-1499-0
2. Jiang WM, Chen X, Wang BJ, Fan ZT, Wu HB (2016) Effects of vibration frequency on microstructure, mechanical properties, and fracture behavior of A356 aluminum alloy obtained by expendable pattern shell casting. Int J Adv Manuf Technol 83:167–175. doi:10.1007/s00170-015-7586-0
3. Kaur P, Dwivedi DK, Pathak PM (2012) Effects of electromagnetic stirring and rare earth compounds on the microstructure and mechanical properties of hypereutectic Al–Si alloys. Int J Adv Manuf Technol 63:415–420. doi:10.1007/s00170-012-3921-x
4. Wang YC, Li DY, Peng YH (2007) Numerical simulation of low pressure die casting of magnesium wheel. Int J Adv Manuf Technol 32:257–264. doi:10.1007/s00170-005-0325-1
5. Jiang WM, Fan ZT, Dai YC, Li C (2014) Effects of rare earth elements addition on microstructures, tensile properties and fractography of A357 alloy. Mater Sci Eng A 597:237–244. doi:10.1016/j.msea.2014.01.009
6. Chung IG, Bolouri A, Kang CG (2012) A study on semisolid processing of A356 aluminum alloy through vacuum-assisted electromagnetic stirring. Int J Adv Manuf Technol 58:237–245. doi:10.1007/s00170-011-3376-5
7. Chandrashekar T, Muralidhara MK, Kashyap KT, Raghothama Rao P (2009) Effect of growth restricting factor on grain refinement of aluminum alloys. Int J Adv Manuf Technol 40:234–241. doi:10.1007/s00170-007-1336-x
8. Kim JK, Yu TX (1997) Forming and failure behaviour of coated, laminated and sandwiched sheet metals: a review. J Mater Process Technol 63:33–42. doi:10.1016/S0924-0136(96)02596-4
9. Wang TM, Liang CH, Chen ZN, Zheng YP, Kang HJ, Wei W (2014) Development of an 8090/3003 bimetal slab using a modified direct-chill casting process. J Mater Process Technol 214:1806–1811. doi:10.1016/j.jmatprotec.2014.03.029
10. Kim J, Lee KS, Kwon YN, Lee B, Chang YW, Lee S (2015) Improvement of interfacial bonding strength in roll-bonded Mg/Al clad sheets through annealing and secondary rolling process. Mater Sci Eng A 628:1–10. doi:10.1016/j.msea.2015.01.035
11. Islam MR, Ishak M, Shah LH, Idris SR, Meriç C (2016) Dissimilar welding of A7075-T651 and AZ31B alloys by gas metal arc plug welding method. Int J Adv Manuf Technol. doi:10.1007/s00170-016-8993-6
12. Jafarian M, Khodabandeh A, Manafi S (2015) Evaluation of diffusion welding of 6061 aluminum and AZ31 magnesium alloys without using an interlayer. Mater Des 65:160–164. doi:10.1016/j.matdes.2014.09.020
13. Zhao Y, Lu ZP, Yan K, Huang LZ (2015) Microstructural characterizations and mechanical properties in underwater friction stir welding of aluminum and magnesium dissimilar alloys. Mater Des 65:675–681. doi:10.1016/j.matdes.2014.09.046
14. Tabasi M, Farahani M, Besharati Givi MK, Farzami M, Moharami A (2016) Dissimilar friction stir welding of 7075 aluminum alloy to AZ31 magnesium alloy using SiC nanoparticles. Int J Adv Manuf Technol 86:705–715. doi:10.1007/s00170-015-8211-y
15. Mofid MA, Abdollah-Zadeh A, Gür CH (2014) Investigating the formation of intermetallic compounds during friction stir welding of magnesium alloy to aluminum alloy in air and under liquid nitrogen. Int J Adv Manuf Technol 71:1493–1499. doi:10.1007/s00170-013-5565-x
16. Zhao Y, Jiang S, Yang SF, Lu ZP, Yan K (2016) Influence of cooling conditions on joint properties and microstructures of aluminum and magnesium dissimilar alloys by friction stir welding. Int J Adv Manuf Technol 83:673–679. doi:10.1007/s00170-015-7624-y
17. Sun M, Niknejad ST, Gao H, Wu L, Zhou Y (2016) Mechanical properties of dissimilar resistance spot welds of aluminum to magnesium with Sn-coated steel interlayer. Mater Des 91:331–339. doi:10.1016/j.matdes.2015.11.121
18. Manladan SM, Yusof F, Ramesh S, Fadzil M (2016) A review on resistance spot welding of magnesium alloys. Int J Adv Manuf Technol 86:1805–1825. doi:10.1007/s00170-015-8258-9
19. Shang J, Wang KH, Zhou Q, Zhang DK, Huang J, Li GL (2012) Microstructure characteristics and mechanical properties of cold metal transfer welding Mg-Al dissimilar metals. Mater Des 34:559–565. doi:10.1016/j.matdes.2011.05.008
20. Gao M, Mei SW, Li XY, Zeng XY (2012) Characterization and formation mechanism of laser-welded Mg and Al alloys using Ti interlayer. Scr Mater 67:193–196. doi:10.1016/j.scriptamat.2012.04.015
21. Dziadoń A, Mola R, Błaż L (2016) The microstructure of the surface layer of magnesium laser alloyed with aluminum and silicon. Mater Charact 118:505–513. doi:10.1016/j.matchar.2016.06.034
22. Hajjari E, Divandari M, Razavi SH, Homma T, Kamado S (2012) Microstructure characteristics and mechanical properties of Al 413/Mg joint in compound casting process. Metall Mater Trans A 43:4667–4677. doi:10.1007/s11661-012-1296-0
23. Jiang WM, Fan ZT, Liao DF, Dong XP, Zhao Z (2010) A new shell casting process based on expendable pattern with vacuum and low-pressure casting for aluminum and magnesium alloys. Int J Adv Manuf Technol 51(1–4):25–34. doi:10.1007/s00170-010-2596-4
24. Geffroy P, Lakehal M, Goñi J, Beaugnon E, Silvain J (2009) Thermal and mechanical behaviour of grey cast iron and ductile iron castings using magnetic molding and lost foam processes. J Mater Process Technol 209:4103–4111. doi:10.1016/j.jmatprotec.2008.10.002
25. Charchi A, Rezaei M, Hossainpour S, Shayegh J, Falak S (2010) Numerical simulation of heat transfer and fluid flow of molten metal in MMA–St copolymer lost foam casting process. J Mater Process Technol 210:2071–2080. doi:10.1016/j.jmatprotec.2010.07.028
26. Jiang WM, Fan ZT, Liu DJ, Wu HB (2013) Influence of gas flowrate on filling ability and internal quality of A356 aluminum alloy castings fabricated using the expendable pattern shell casting with vacuum and low pressure. Int J Adv Manuf Technol 67:2459–2468. doi:10.1007/s00170-012-4663-5
27. Liu XJ, Bhavnani SH, Overfelt RA (2007) Simulation of EPS foam decomposition in the lost foam casting process. J Mater Process Technol 182:333–342. doi:10.1016/j.jmatprotec.2006.08.023
28. Shayegh J, Hossainpour S, Rezaei M, Charchi A (2010) Developing a new 2D model for heat transfer and foam degradation in EPS lost foam casting (LFC) process. Int Commun Heat Mass 37:1396–1402. doi:10.1016/j.icheatmasstransfer.2010.07.015

29. Emami SM, Divandari M, Hajjari E, Arabi H (2013) Comparison between conventional and lost foam compound casting of Al/Mg light metals. Int J Cast Metal Res 26:43–50. doi:10.1179/1743133612Y.0000000037
30. Guler KA, Kisasoz A, Karaaslan A (2014) Fabrication of Al/Mg bimetal compound casting by lost foam technique and liquid-solid process. Mater Test 56:700–702. doi:10.3139/120.110624
31. Jiang WM, Fan ZT, Li GY, Yang L, Liu XW (2016) Effects of melt-to-solid insert volume ratio on the microstructures and mechanical properties of Al/Mg bimetallic castings produced by lost foam casting. Metall Mater Trans A. doi:10.1007/s11661-016-3788-9
32. Hajjari E, Divandari M, Razavi SH, Emami SM, Homma T, Kamado S (2011) Dissimilar joining of Al/Mg light metals by compound casting process. J Mater Sci 46:6491–6499. doi:10.1007/s10853-011-5595-4
33. Jiang WM, Li GY, Fan ZT, Wang L, Liu FC (2016) Investigation on the interface characteristics of Al/Mg bimetallic castings processed by lost foam casting. Metall Mater Trans A 47:2462–2470. doi:10.1007/s11661-016-3395-9
34. Hajjari E, Divandari M, Razavi SH, Homma T, Kamado S (2012) Intermetallic compounds and antiphase domains in Al/Mg compound casting. Intermetallics 23:182–186. doi:10.1016/j.intermet.2011.12.001